Load distribution and tooth root stress of highly crowned spherical gear couplings working at high misalignment angles

Aurea Iñurritegui[a,*], Jon Larrañaga[a], Aitor Arana[a], Ibai Ulacia[a]

[a]*Mondragon Unibertsitatea, Department of Mechanical and Industrial Production, Arrasate-Mondragon, Pais Vasco, SPAIN*

Abstract

Spherical gear couplings are commonly used mechanical components to transmit power between highly misaligned rotating shafts. For that, gear couplings are manufactured with high longitudinal crowning and are usually small due to space restrictions, with the probability to contain undercutting sections. High misalignment angles cause the number of teeth in contact to decrease drastically, resulting in the failure of the component by tooth root fatigue breakage.

This paper investigates the load distribution and the tooth root stress of highly crowned spherical gear couplings working at high misalignment angles using a finite element model. Moreover, a deep understanding of the bending tooth root stresses in terms of the operating conditions is presented, which is novel for such high misalignment angles ($\gamma \geq 3°$). Results show that different mechanical behaviors are observed at low or high misalignment angles since teeth in the pivoting position lose contact. This results in a tooth root stress history change from a sinusoidal cycle to a pulsating cycle. Finally, this study shows evidence that current sizing methods are not suitable, and underlines the need for further research to determine the spherical gear coupling life to tooth root bending fatigue.

Keywords: spherical gear coupling, high misalignment, load distribution, tooth root bending stress, Finite Element Method

*Corresponding author
Email address: ainurritegui@mondragon.edu (Aurea Iñurritegui)

Nomenclature

A	coefficient to comprise the variables related to the geometry in tooth root stress
b	face width of the gear coupling
b_{eff}	effective face width of the gear coupling
C	number of teeth in contact
C_{eff}	number of effective teeth in contact
d_p	pitch diameter of the gear coupling
e	thickness of the tooth surface with smaller mesh elements
F_{CN}	total contact normal force
j_n	normal clearance
K	coefficient to comprise the rest of the coefficients affecting tooth root stress
k_F	overload coefficient
k_{ls}	load sharing factor
k_m	load distribution factor
LD_{z_i}	load distribution in each tooth z_i
m_n	normal module
n_{z_i}	total contact nodes in each tooth z_i
r_c	crowning radius of the hub
Y	lewis factor
z	total number of teeth in the gear coupling
α	pressure angle
Γ	applied torque
γ	misalignment angle
$\delta_{\max}$	maximum displacement of the contact point from the reference section along the face width
θ_i	angular position of the hub
σ	tooth root bending stress

1. Introduction

Spherical gear couplings are mechanical components used to transmit power between misaligned shafts. They are preferred over other non-splined connections, due to their high power density and capacity to accommodate angular misalignments [1, 2]. For example, they are used in sheet metal rolling mills [3, 4, 5], where high misalignment angles ($\gg 3^\circ$) are required due to the reduced space between rollers.

They are composed of a highly crowned toothed hub (external part) and a commonly straight sleeve (internal part) [6, 7], both of which have the same number of teeth. For the generation of highly crowned surfaces of the hub, it is necessary to consider the threaded surface of the generating hob and the kinematics of the hobbing process. Indeed, it is likely that undercutting sections appear, as previously shown by the authors in [8].

The most common use of gear couplings is in applications where slight misalignment occurs. Damage occurring as a result of surface wear [9, 10, 11, 12] caused by improper lubrication represents 75% of all gear coupling failures [13, 14]. Low misalignment angles decrease the longitudinal sliding between the hub and the sleeve, which leads to fretting damage on the surface [15, 16, 17]. The next most common failure stems from misalignment (20%), which leads to tooth root breakage failure [18]. Moreover, this latter is significantly increased in highly crowned spherical gear couplings, as undercutting sections are more frequent [5, 8].

Works in the literature have shown the relationship between the design parameters and the misalignment angle [19]. Indeed, they have shown that an adequate selection of the number of teeth, the pressure angle, and the crowning ratio, among others, can produce a spherical gear coupling design that can achieve misalignment angles greater than 15°. Nevertheless, existing works for sizing and designing gear couplings [14, 20, 21, 22, 23, 24, 25] are mainly focused on low misalignment angles, and spherical gear couplings for high misalignment applications are referred to as special cases. The equations from the cited works are derived from gear tooth root bending calculations and all have the same structure represented in Eq. (1).

$$\sigma = \frac{\Gamma \cdot K}{A} k_m \cdot k_{ls} \tag{1}$$

where, Γ is the applied torque, A is a coefficient to include the geometrical variables to represent the moment of inertia and resistant section of the tooth (e.g., the module m_n, the pitch diameter d_p, the face width b...). Likewise, K is a factor to include all the coefficients which influence tooth root stresses (e.g., the application factor k_a, the quality coefficient Z_Q...). Two relevant coefficients for spherical gear coupling are remarked to account for the number of teeth in contact (k_{ls}) and the effective face width (k_m) supporting the load.

On the one hand, the load distribution factor (k_m) considers the length of the face width actually carrying the load. In ideal aligned conditions, all the teeth are engaged and contact is centered on the face width [26]. When slight misalignment occurs, however, the spatial motion becomes complex and the relative position between both hub and sleeve differs depending on the meshing position [25, 27, 28]. The relative motion between hub and sleeve is made up of pivoting (swinging) and tilting movements, and the contact pattern and position changes accordingly, presenting a lemniscata shape [8, 29, 30, 31]. The evolution of the contact point caused by the misalignment angle results in a variation of the effective face width supporting the load [27]. Some works in the literature [11, 32] propose an Eq. (2) to determine the maximum contact point displacement ($\delta_{\max}$), and then define the portion of the tooth supporting the load. However, very little data exists related to the effective face width, and how to consider it in high misalignment applications [20, 22, 33].

$$\delta_{\max} = r_c \sin(\gamma) \cos\left(2\pi \frac{z_i}{z}\right) \tag{2}$$

where, r_c is the crowning radius, γ is the misalignment angle, z is the total number of teeth, and z_i is the position of each tooth.

On the other hand, the load sharing factor (k_{ls}) is used to account for the number of teeth actually carrying the load. Indeed, the tilting position (in the perpendicular plane to the misalignment angle) is the most critical one, because teeth in this angular position are the first to come into contact. As they have the smallest clearance value [8, 29], they suffer the highest stresses [34]. Torque value, associated with the available clearance, makes the gear coupling stiffness vary [35], and increase as the number of teeth in contact rises. However, if manufacturing errors occur, clearance will no longer be constant. For this reason, Beckmann [23] also includes a coefficient to account for the manufacturing quality and its effect on the number of teeth in contact. Indeed, indexing errors can imply an increase of 22% in the stress values supported by the gear coupling [23]. On top of that, the non-uniformity of load distribution will be increased [36, 37, 38].

In the presence of low misalignment angles, gear couplings have already shown a non-uniform load distribution [11, 26, 30, 39]. That is why, efforts have been focused on the increase of the contact surface to reduce stresses and obtain more uniform load distribution by modifying the longitudinal amount of crowning [28, 40, 41].

The majority of works published in the literature only focus on the effect of the misalignment angle ($\gamma \leq 1.5°$) on the number of teeth in contact [1, 14, 24, 28, 36, 42]. However, these values were not experimentally validated and loading conditions were not considered. As a consequence, commonly used conservative criteria in gear coupling sizing is to assume that half of the teeth are carrying the load [14, 22, 24]. Nevertheless, it has been shown that tooth stiffness and torque have a significant impact [5, 39], thus, it is expected that this criterion will oversize the part to a great extent depending on the geometry of the gear coupling or the working conditions.

Due to the complex kinematics of misaligned gear couplings, and the effect of multiple variables, analytical models exist to analyze the influence of each of the variables individually; e.g., clearance distribution [29, 31, 43] or load distribution [11, 44], among others. However, it is known that parameters are interrelated and that they cannot be independently analyzed, especially when high misalignment angles are present. That is why, recently, the use of finite element models has grown. 2D models have been used to determine load distribution and the number of teeth in contact under different loading conditions [45] or under the effect of pitch errors [46]. However, to analyze the effect of the misalignment angle 3D models are required [47, 48, 49]. Moreover, the accuracy of the geometry has shown to have a great influence on the non-loaded tooth contact analysis (NLTCA) resulting from the small crowning radius and the appearance of undercutting sections [8]. That is why it is expected to be of relevance in the loaded tooth contact analysis (LTCA) due to the possible stress concentrations. For instance, Guan et al. [30] presented the

evolution of the load distribution with misalignment angles up to $\gamma = 0.2°$ while showing high risk of tip edge contact due to the misalignment angle.

From the literature review, it can be confirmed that the number of teeth in contact and the contact position significantly vary in terms of low misalignment angles. This variation affects the load distribution, and consequently the tooth root stress distribution. The complex mechanical behavior and the complexity of the geometry itself (presence of undercutting sections) make FE models a very suitable tool for the analysis. However, the works cited earlier are principally focused on misalignment angles below one degree. Thus, the behavior at higher misalignment angles is uncertain, and the application of current sizing criteria to determine load distribution and maximum tooth root stresses can result in over sizing, or even what may be more critical, under sizing of the component.

Therefore, this paper numerically determines the load distribution and the tooth root stress behavior of a highly crowned spherical gear coupling working at high misalignment angle applications, considering the variation of the contact position and the number of teeth in contact. To this end, the main goals of this research are:

(1) To develop a finite element model, based on the mathematical geometry generation model (already presented in [8]) for spherical gear couplings working in high misalignment applications. This model will be capable of accurately representing all the geometry features of spherical gear couplings, such as undercutting sections.

(2) To analyze the influence of the misalignment angle, specially $\gamma \gg 1.5°$, and the applied torque on the number of teeth in contact, the load distribution, and the tooth root stress.

2. Geometry of the spherical gear coupling tooth surfaces

The main tooth modification employed in spherical gear couplings is longitudinal crowning or barreling [5, 29, 50, 51, 19] to achieve a more uniform contact pressure distribution and to prevent the undesired edge contacts caused by slight misalignments during operation or assembly.

Barreling involves a tooth thickness variation in the hub tooth surfaces and a tooth clearance change along the face width [29, 51]. In the reference section, the tooth thickness is the greatest, and a constant clearance between the hub and the sleeve tooth active profiles can be observed in aligned conditions (Fig. 1(a)). From the literature [8, 52], it is known that contact moves further away from the central section when misalignment is present, thus, longitudinal crowning and clearance distribution will lead to different contact conditions. Indeed, as the section moves further away, the hub tooth surfaces will no longer conform nominally to the tooth surface of the sleeve [16, 36] (Fig. 1(a)).

As shown in Fig. 1(b.1), the whole active involute tooth surfaces are in contact in aligned (A) and loaded conditions without tip relief, because of the constant clearance between the hub and the sleeve tooth surfaces. However, in tooth sections further away from the central section (misaligned conditions, M), the non-constant variation of the clearance value will cause tip edge contact between the fillet tooth surface of the sleeve and the tip edge tooth surface of the hub, resulting in high contact pressure values. To avoid it, in this research, the hub and sleeve tooth surfaces are generated with a chamfer tip relief to center the contact on the active tooth profile, as shown in Fig. 1(b.2). It is already known that tip relief modification has an effect on load distribution of spur gears [53, 54], that is why for this research the lowest possible tip chamfer was considered to avoid edge contact in the analyzed working conditions.

For this purpose, the generating rack cutter tooth surface is modified by a linear tip-relief (enlarged for clarity in Fig. 2) which is defined in coordinate system S_a as follows:

$$\mathbf{r}_{\mathrm{a}}(u) = \begin{cases} \text{if } u_{\mathrm{lim}} < u \leq u_{\mathrm{max}} & [u \quad 0 \quad 0 \quad 1]^{\mathrm{T}} \\ \text{if } u_{\mathrm{min}} \leq u \leq u_{\mathrm{lim}} & [u \quad -(u + u_{\mathrm{lim}}) \sin(\alpha_{\mathrm{ch}}) \quad 0 \quad 1]^{\mathrm{T}} \end{cases} \tag{3}$$

where u_{lim} is the active profile limit from which the chamfer is defined and α_{ch} is the chamfer angle. In this research, $u_{\mathrm{lim}} = 0.3$ and $\alpha_{\mathrm{ch}} = 3.5°$ are considered. Further research would be required to optimize the value or analyze the influence of different types of tip reliefs, but it is out of the scope of this paper.

The hub and sleeve tooth surfaces are generated considering the manufacturing method, the meshing theory, and the double-enveloping process [55] defined in-depth by the authors in [8]. Fig. 2 provides an overview of the generation of the hub (lower part) and the sleeve (upper part), starting from the rack-cutter tooth surface with tip relief.

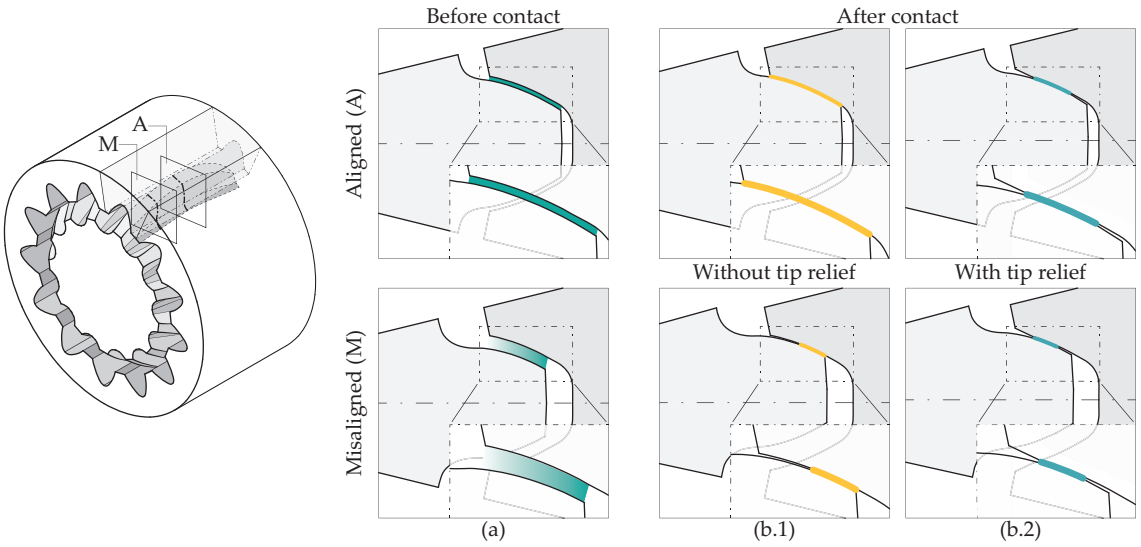

Figure 1: (a) clearance and (b) contact conditions of spherical gear couplings in aligned (b.1) and misaligned (b.2) working conditions, showing the benefit of applying the tip relief.

In the case of the hub, a hob thread surface Σ_w is generated as the cutting tool from the generating rack-cutter tooth surface Σ_c. This follows a circular feeding motion which determines the hub tooth surface Σ_h as the envelope to the family of surfaces of the hob. The hob thread surface is determined from the rack-cutter tooth surface Σ_c considering the meshing equation (5). The hub tooth surface is then generated by coordinate transformation (4) from system S_c to system S_h, taking into consideration the double-enveloping process [55] with two independent parameters of generation ϕ_w and s_w (6, 7).

$$\mathbf{r}_h(u, v, \psi_w, s_w, \phi_w) = \mathbf{M}_{hw}(s_w, \phi_w)\,\mathbf{M}_{wc}(\psi_w)\,\mathbf{r}_c(u, v) \tag{4}$$

$$f_1(u, v, \psi_w) = \left(\frac{\partial \mathbf{r}_w}{\partial u} \times \frac{\partial \mathbf{r}_w}{\partial v}\right) \cdot \frac{\partial \mathbf{r}_w}{\partial \psi_w} = 0 \tag{5}$$

$$f_2(u, v, s_w, \phi_w) = \left(\frac{\partial \mathbf{r}_h}{\partial u} \times \frac{\partial \mathbf{r}_h}{\partial v}\right) \cdot \frac{\partial \mathbf{r}_h}{\partial \phi_w} = 0 \tag{6}$$

$$f_3(u, v, s_w, \phi_w) = \left(\frac{\partial \mathbf{r}_{h,a}}{\partial u} \times \frac{\partial \mathbf{r}_h}{\partial v}\right) \cdot \frac{\partial \mathbf{r}_h}{\partial s_w} = 0 \tag{7}$$

Here, ψ_w is the generation parameter for the hob thread surface, and matrices $\mathbf{M}_{hw}$ and $\mathbf{M}_{wc}$ are the coordinate transformation matrix [8].

As regards the sleeve, a shaper Σ_s is generated as the cutting tool from the generating rack-cutter tooth surface, with the meshing equation (9). This follows a straight tool path to determine the tooth surfaces of the sleeve Σ_g, as the envelope to the family of surfaces of the shaper. Coordinate transformation (8) from system S_c to system S_g and consideration of the meshing equations (10) by parameter ψ_s enables to determine the sleeve tooth surface.

$$\mathbf{r}_g(u, v, \psi_s, \phi_s) = \mathbf{M}_{gs}(\phi_s)\,\mathbf{M}_{sc}(\psi_s)\,\mathbf{r}_c(u, v) \tag{8}$$

$$f_4(u, v, \psi_s) = \left(\frac{\partial \mathbf{r}_s}{\partial u} \times \frac{\partial \mathbf{r}_s}{\partial v}\right) \cdot \frac{\partial \mathbf{r}_s}{\partial \psi_s} = 0 \tag{9}$$

$$f_5(u, v, \psi_s, \phi_s) = \left(\frac{\partial \mathbf{r}_g}{\partial u} \times \frac{\partial \mathbf{r}_g}{\partial v}\right) \cdot \frac{\partial \mathbf{r}_g}{\partial \phi_s} = 0 \tag{10}$$

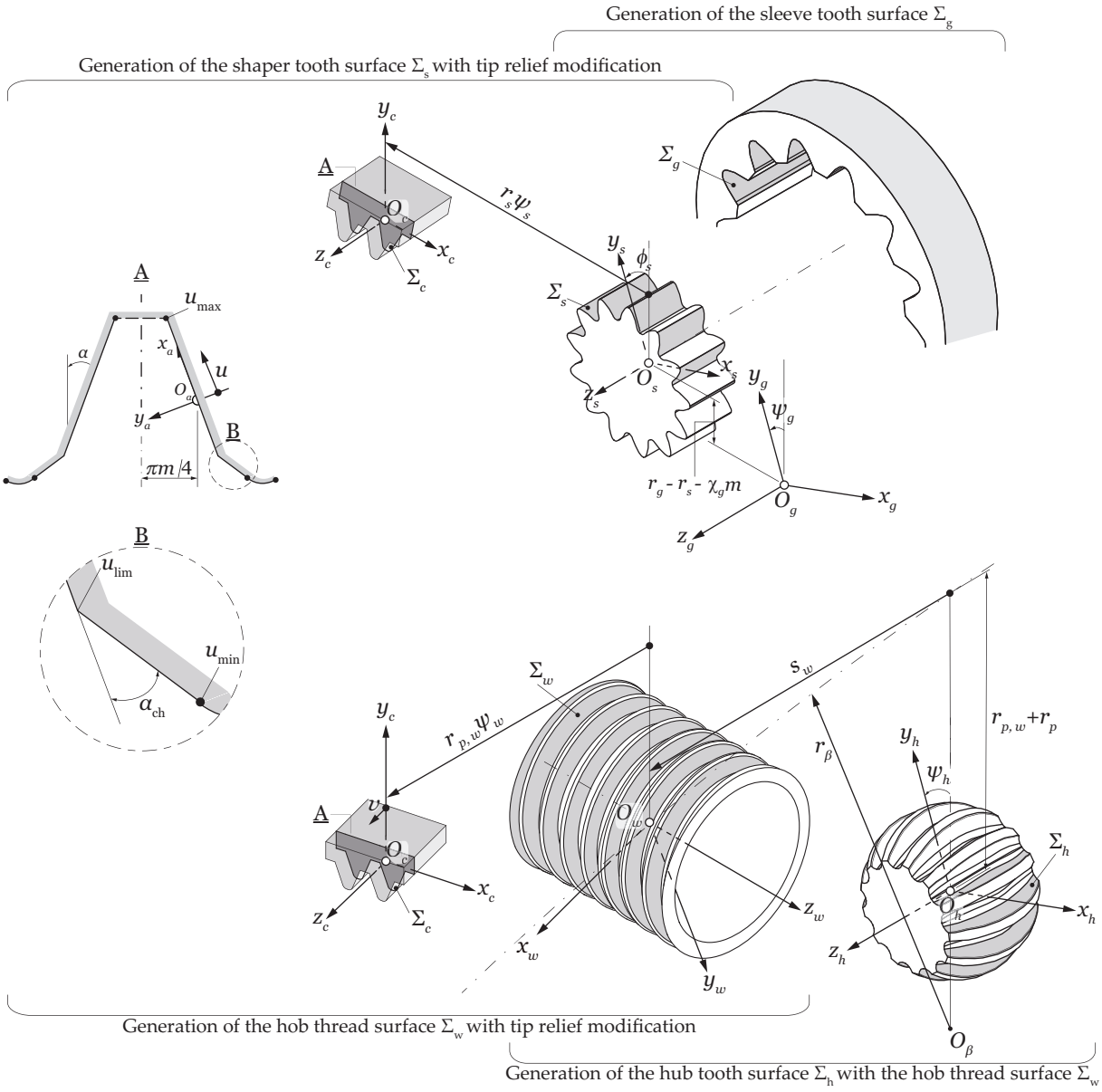

Figure 2: Derivation of the hub tooth surface Σ_h and sleeve tooth surface Σ_g with linear tip relief, with the prior determination of the hob thread surface Σ_w and shaper tooth surface Σ_s.

3. Definition of spherical gear couplings finite element model

The FE method is employed to simulate the contact path and mechanical behavior of spherical gear couplings. Compared to other analytical methods, this approach has the advantage of taking into account the effects derived from the elastic deformations of all the teeth in the gear coupling and body, including tooth stiffness, tilting-moment effect generated by misalignment, and modifications of the load-sharing between the teeth.

3.1. Mesh

The meshing of the hub and sleeve is based on the method proposed in [56], which is commonly employed for gear analysis. This well-known meshing procedure produces a uniform structured mesh over the gear geometries,

dividing the teeth into five sections: right and left active and fillet profiles of the gear tooth, and the gear body.

The mesh is produced automatically from the generated geometry using the generation model described in section 2. Fig. 3(a) shows a detailed view of the hexahedral element mesh in the hub. The same meshing technique is employed in the sleeve. The mesh is developed with the aim of capturing tooth root stresses, and with a non refined mesh in the contact zone of the teeth. This stems from the main objective of this study, which is the analysis of tooth root stress distribution. The novelty of the meshing employed for spherical gear couplings in this paper compared to the methodologies commonly used [47, 48, 49], lies in a finer mesh in the tooth root region below the potential contact zone region. This provides smaller elements in those zones with higher stress gradients without increasing the number of elements, and thus the computational cost. Fig. 3(a) depicts: (i) a fine mesh across the contact area of the gear coupling, and (ii) a coarser mesh that transitions from the fine mesh up to the hub (or sleeve) edges with a bias factor. The finer mesh region is delimited for each misalignment angle by a NLTCA [8], plus an additional 25% as commonly done for spur gears.

Additionally, Fig. 3(b) illustrates the transverse meshing employed for the hub and sleeve teeth composed of: (iii) a reduced mesh in the root and flank and a coarser mesh in the body of the teeth, where stress gradients are smaller. Moreover, this mesh comprises several layers of smaller elements near the surface of the flank and fillet regions, characterized by thickness $e = 0.15m_n$ [57]. The refined mesh between the surface layer and the body is generated with a bias factor for a smoother transition.

The element size in the contact zone and the fillet of the hub is of 0.08 mm.

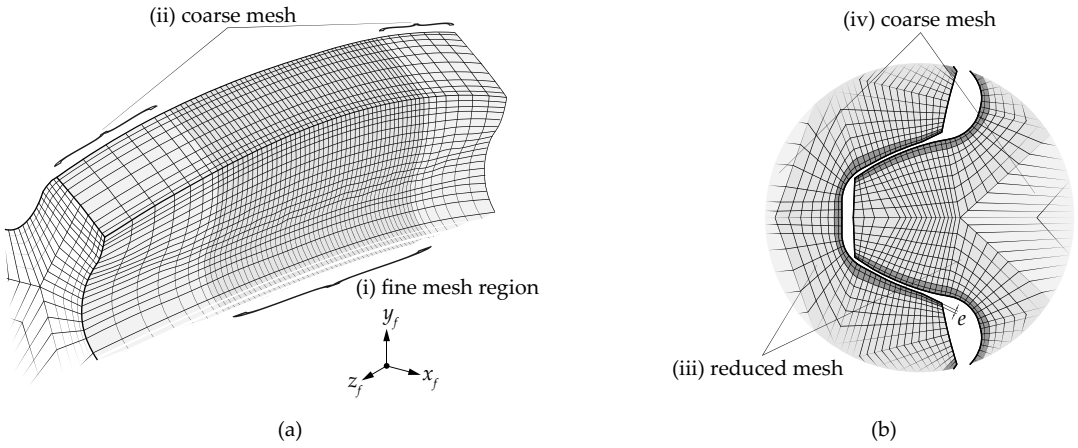

Figure 3: Finite element mesh: (a) hub longitudinal mesh discretization with a (i) fine mesh in the potential contact zone and tooth root, and (ii) a coarser mesh up to the edges; and (b) detail of the hub and sleeve teeth transversal mesh with a (iii) reduced mesh in the tooth comprising a non-biased contact layer, and a (iv) coarse mesh in the body part.

3.2. Model assembly

Fig 4(a) shows a fixed coordinate system S_f where the hub and sleeve geometries are assembled. An auxiliary system S_m is defined parallel to S_f and enables the misalignment of the sleeve around axis x_m, while it remains fixed during the analysis. The origin (O_f, O_m) of coordinate systems S_f and S_m is located in the central section of the gear coupling (0,0,0).

The hub and sleeve models are defined in coordinate systems S_1 and S_2, respectively. The nodes located on the inner hub radius and the external rim of the sleeve form rigid surfaces. These surfaces are represented in yellow and green, in Fig 4(b). A hub reference node O_1 is defined at the origin of system S_1 and is rigidly connected to its corresponding rigid surface while allowing rigid body motion between the reference node and the rigid surface. The same procedure is followed for the sleeve reference node O_2 and the external rim rigid surface in the coordinate system S_2. The assembly of system S_2 in the auxiliary coordinate system S_m is made with the misalignment angle around axis x_m. In consequence, the characteristic positions of the gear coupling will be defined as follows: (i) pivoting position, $\pi/2$ rad and $3\pi/2$ rad, parallel to the misalignment axis and, (ii) tilting position, 0 rad and π rad, perpendicular to the misalignment axis.

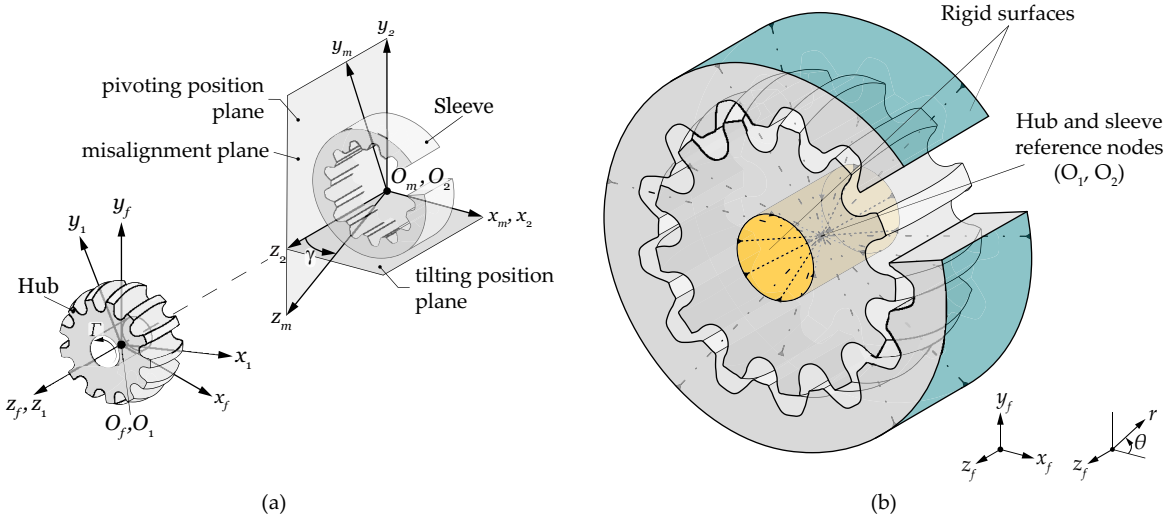

Figure 4: Description of the spherical gear coupling finite element model for the loaded tooth contact analysis: (a) coordinate system for the model assembly, and (b) definition of rigid surfaces and reference nodes.

To carry out the FE analysis and ensure suitability for post-processing, a cylindrical coordinate system (r, θ, z_f) is defined, as shown in Fig 4(b).

In real working conditions, the spherical gear coupling is connected to a shaft at its ends. This generates the load distribution to be delocalized along the face width. Moreover, maximum tooth root stresses will also increase due to the bending moments generated by the shaft [32]. As the main objective of this research is to explain the mechanical behavior of highly crowned spherical gear couplings, the shaft to which the hub or sleeve is connected is not considered. This also suppresses the effect of the shaft on the load distribution. Hence, any non-symmetry of the load distribution will be related to the contact position and the effect of the working conditions (torque and/or misalignment).

3.3. Load cases and boundary conditions

Each simulation is carried out at a certain angular position along the meshing line (Fig. 4). The degrees of freedom of the sleeve reference node are blocked. Torque Γ is applied through the released degree of freedom of the hub reference node around axis z_1 (Fig 4(a)). The rest of the degrees of freedom of the hub reference node are also blocked.

Node-to-segment contact pairs are specified between the teeth of the hub and the sleeve. Friction can be considered in the tangential behavior of the contact, however, it is out of the scope of this research and has not been included. During the contact process, it is unlikely that a node makes exact contact with the surface, and for that reason, a contact tolerance is associated with each surface. If a node is within the contact tolerance, it is considered to be in contact with the segment. In this analysis, a tolerance value of $1/20$ of the smaller element size was selected, centered on both sides of the segment (Fig. 5(b)).

A linear elastic material is defined for the model, under the assumption that the deformations are so small that they may be studied under the small strains theory. The element type considered for the analysis is a first-order isoparametric hexahedral element (type 7 [58]).

3.4. Post-processing of the results

3.4.1. Contact pattern and number of teeth in contact

To determine the contacting teeth, the contact status output [58] is extracted from the traction active profile nodes of the hub. An indicator for contact is recognized by a congruent representation of the contact status output in the master and slave contact bodies, as depicted in Fig. 5(a). These positions are then replaced by the centroid of all the nodes in contact in each tooth, for comparison in the contact pattern graphs. Throughout the simulation and the

iterative process, the motion of the nodes is checked to verify whether the nodes are near a segment or not, considering the contact tolerance as defined in Fig. 5(b).

It is important to note at this point, that the values of the centroid and contact position are dependent on the mesh size and the contact tolerance employed in the simulation, as the information is extracted from the position of the nodes. Nevertheless, the mesh used in this research is sufficient to analyze the evolution of the contact pattern and the influence of the operating conditions.

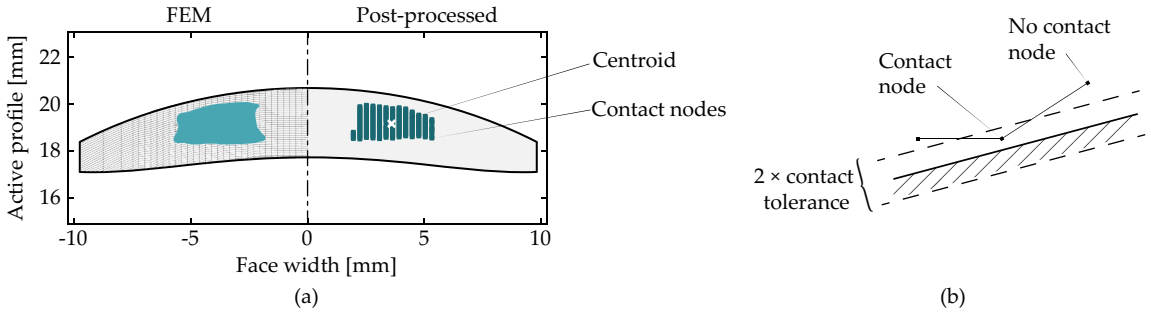

Figure 5: Contact nodes definition: (a) contact status output from FE solver and post-processed contact nodes and centroid, and (b) check of node contact with the contact tolerance definition (adapted from [58]).

3.4.2. Load distribution

The load distribution for each tooth is obtained by the summation of the contact normal force (F_{CN}) of the nodes in contact (Eq. (11)). Once calculated, the contact normal force is divided by the total normal force applied to the whole gear coupling to obtain the load distribution, as shown in Eq. (12).

$$F_{CN,z_i}(\xi) = \sum_{n=1}^{n_{z_i}} F_{CN}(n) \tag{11}$$

$$LD_{z_i}(\xi) = \frac{F_{CN,z_i}(\xi)}{\sum_{z_i=1}^{z} F_{CN,z_i}(\xi)} \tag{12}$$

where, F_{CN,z_i} corresponds to the total contact normal force for tooth z_i at increment ξ, n_{z_i} refers to the total contact nodes in each tooth z_i, and LD_{z_i} is the load distribution of each tooth.

3.4.3. Tooth root stresses

Tooth root stresses are obtained in every element of the fillet region of the traction part of each tooth (Fig. 6(a)). Although compression side root stresses are higher than those from the traction side [20, 59, 60], only the traction side stresses were analyzed as these are critical for tooth root fatigue life.

The component of the stress tensor reflecting the bending stress of the gear hub is the stress value analyzed in this work, i.e. the component in the transverse direction to the tooth. For this reason, the bending direction corresponds to $\sigma_{22} = \sigma_{\theta\theta}$, taking into account the cylindrical coordinate system in which the model is built (Fig. 4(b)).

The stiffness of the hexahedron element type employed in the model is formed using eight Gaussian integration points (type 7 in Marc solver [58]). To this end, as depicted in Fig. 6(a), stress values in each element are calculated at every integration point of the hexahedral element. Nodal values are then obtained by interpolating those values linearly from the element surface integration points to the nodes of the element [58] (Fig. 6(b)).

Tooth root stresses are calculated in all the teeth (Fig. 7(a)), however, due to the high mesh density and complex geometry, values are still difficult to see without the mesh (Fig. 7(b)). That is why traction side teeth projections are illustrated in this research as shown in Fig. 7(c). Here, the tilting position tooth root stress distribution is shown in the whole teeth (active profile and root). Moreover, to compare different working conditions the tooth root stress distribution along the face width is represented (the maximum tooth root stress radius), as shown in Fig. 7(d).

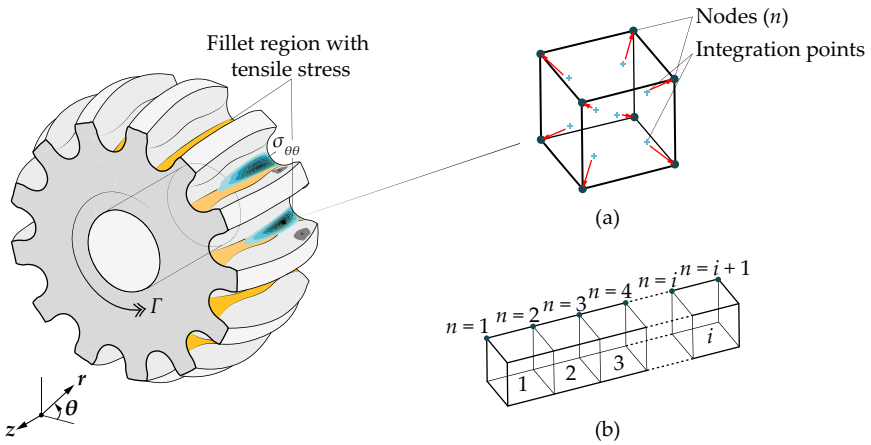

Figure 6: Tooth root stress determination region: (a) nodal stress calculation from FE solver, and (b) representative stress nodal value for each element.

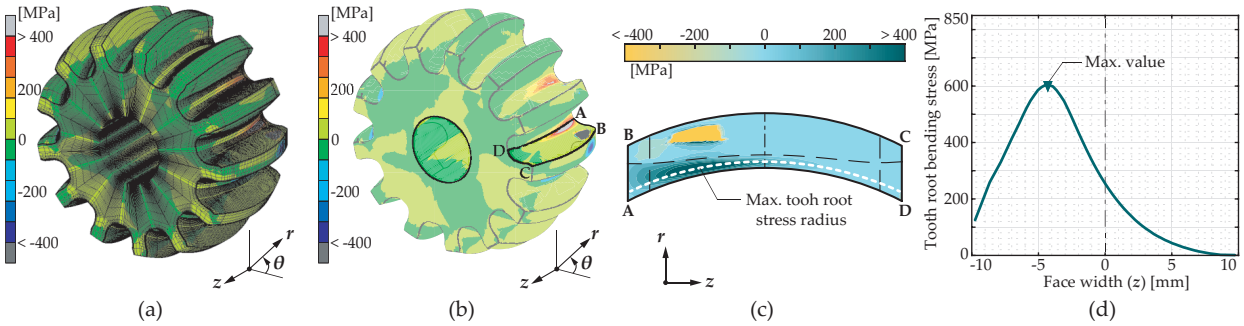

Figure 7: Tooth root stress representation along the research: (a) tooth root bending stress in the whole gear coupling with the FE mesh, and (b) without the mesh, (c) tilting position traction side tooth root stress projection, and (d) maximum tooth root stress radius along the face width.

4. Definition of the case of study and types of analysis

In this research, the behavior of highly crowned spherical gear couplings is analyzed using a geometry with the following distinguishing features, and based on an industrial application of a roll-leveling machine [5, 33]:

- Small pitch diameter.
- Small number of teeth.
- Small crowning radius, which involves a large amount of longitudinal crowning.
- Hub tooth surface with undercut sections due to the small crowning radius.
- High maximum working misalignment angle ($\gamma_{\max} = 7.5°$).

The parameters of the case study are described in Table 1. A common carburized and quenched 15NiCr11 steel is used in the spherical gear coupling model defined by its linear elastic properties (Table 1).

Loaded tooth contact analysis was conducted following the indications of Section 3 in Marc solver [61], a general-purpose FE analysis computer program.

Table 1: Design parameters, operating conditions, and material properties for the highly crowned spherical gear coupling case study.

Parameter	**Case study**
Pitch diameter, d_p [mm]	39
Normal module, m_n [mm]	3
Number of teeth, z [-]	13
Normal pressure angle, α [°]	30
Aspect ratio, b/d_p [-]	0.5
Backlash, j_n [mm]	0.285
Crowning radius, r_c [mm]	24
Misalignment angle, γ [°]	0 - 7.5
Applied torque, Γ [Nm]	0 - 1500
Young's modulus, E [GPa]	210
Poisson coefficient, υ [-]	0.33
Density, ρ [kg/m^3]	7850
Yield stress, σ_y [MPa]	850
Ultimate stress, σ_u [MPa]	1010
Fatigue stress limit, σ_e [MPa]	520

Two types of static simulations were performed, with two different objectives:

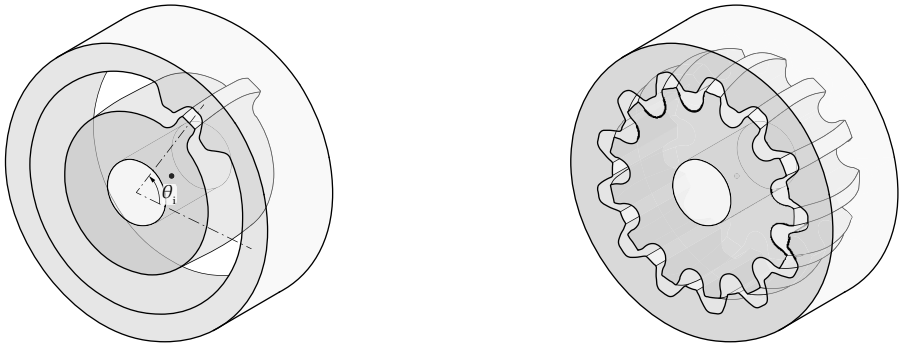

(a) (b)

Figure 8: Types of FE model analysis: (a) single toothed gear coupling, and (b) complete gear coupling.

- Single toothed gear coupling model
  The aim is to understand the evolution of the contact pattern in terms of the angular position when working at high misalignment angles, and its impact on tooth root stresses.

  Without the convective effects of the adjacent teeth, it is analyzed as a function of the applied torque and misalignment angle. The model is composed of a single hub and sleeve tooth at a certain angular position θ_i, as shown in Fig. 8(a). The static analysis is repeated for several angular positions distributed in the cycle of meshing, under the same working conditions. The angular position θ_i of each analysis varies between 0 and $(2\pi - 2\pi/z)$, i.e., $\Delta\theta_i = \pi/9$ rad, with a total of 20 angular positions simulated for each working condition. In each simulation, the contact pattern, and the tooth root stress distribution are obtained directly from the FE solver, with the procedure described in sections 3.4.1 and 3.4.3.

- Complete gear coupling model
  The goal is to understand the load distribution based on the number of teeth in contact, and its effect on the tooth root stress history.

  This is also examined as a function of the applied torque and misalignment angle. The model is composed of all the teeth in the hub and sleeve as depicted in Fig. 8(b). The contact position, the number of teeth in contact, the

load distribution, and the tooth root stress distribution are obtained from the FE solver, following the procedures in sections 3.4.1-3.4.3.

5. Results

5.1. Mechanical behavior of single toothed gear coupling as a function of the angular position

5.1.1. Contact pattern evolution

Fig. 9 shows the active profile of the hub with the contact pattern in terms of the working conditions (Γ and γ). As it can be observed in Fig. 9(a), the contact pattern evolves from a centered and stable position in aligned conditions (point contact), to a wider and longer contact pattern as the misalignment angle increases (lemniscata shape). Indeed, it is observed that the contact amplitude ($\delta_{\max}$) increases, while it remains centered around the reference section of the hub.

In the case of a constant misalignment angle in Fig. 9(b), it can be seen that as torque increases the contact pattern is flattened. However, this has a negligible effect on the amplitude. Moreover, contact is spread over the pitch diameter as load increases, which is consistent with the literature [24, 8]. This confirms that the behavior of highly crowned spherical gear couplings is consistent with them at this point.

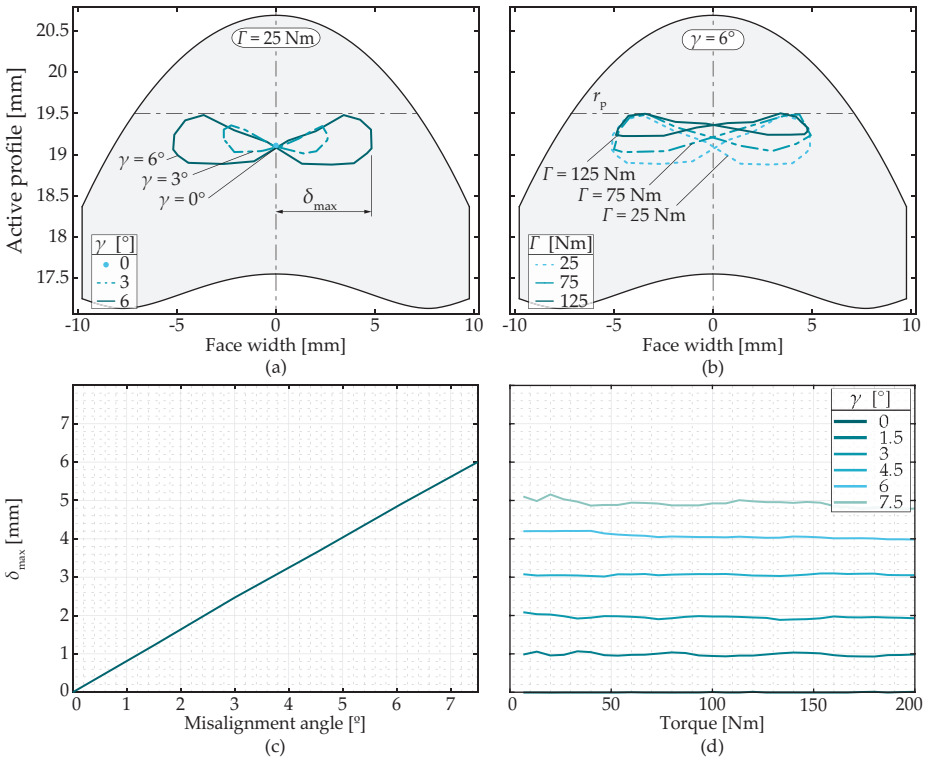

Figure 9: Contact pattern centroid evolution for every angular position and the variation of the maximum displacement of the contact point ($\delta_{\max}$): (a) contact pattern centroid evolution as a function of the misalignment angle for a constant torque applied Γ = 25 Nm, and (b) as a function of the applied torque for a constant misalignment angle $\gamma = 6°$, (c) $\delta_{\max}$ as a function of the misalignment angle, and (d) $\delta_{\max}$ as a function of the applied torque.

The maximum contact displacement from the reference section ($\delta_{\max}$) can be seen in Fig. 9(c) and Fig. 9(d) as a function of the misalignment angle and the applied torque, respectively. These values correspond to the teeth in the tilting angular position, as being the ones with the maximum displacement. It can be seen that the misalignment angle is the main contributor to the variation of the contact position along the face width. The influence of torque arises from the stiffness of the component and is nearly negligible.

5.1.2. Tooth root stress evolution

Fig. 10 shows the maximum tooth root stress distribution along the contact path of the hub at a constant misalignment angle of 6° (Fig. 10(a)). Tooth root stresses in Fig. 10(b) are normalized relative to the maximum tooth root stress value in the pivoting position (Eq. (13)) to depict their variation depending on the contact position along the face width, i.e., angular position.

$$\sigma_{\text{normalized}} = \frac{\sigma}{\sigma_{\text{pivoting}}} \tag{13}$$

It is observed that the maximum value of the tooth root stress along the face width is positioned right at the contact section. Moreover, this position evolves together with the contact pattern, that is, it is shifted from the reference section as the contact displaces. It can also be seen that tooth root stresses increase up to 10% from the pivoting position (contact in the reference section) to the tilting position (most displaced contact point). This demonstrates that tooth geometry and stiffness affect tooth root stresses in misaligned conditions, regardless of the load distribution. The slight non-symmetry of tooth root stress in symmetrical angular positions is linked to the twist-effect phenomena present in highly crowned hub tooth surfaces [8].

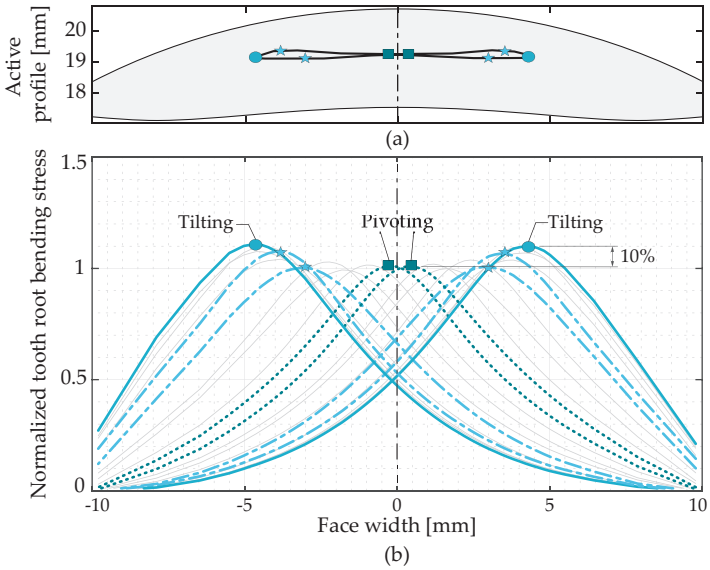

Figure 10: (a) contact pattern centroids, and (b) maximum tooth root stress distribution along the face width according to the angular position for $\Gamma = 100$ Nm and $\gamma = 6°$.

5.2. Mechanical behavior of complete gear coupling as a function of the misalignment angle and torque

5.2.1. Stiffness

Fig. 11(a) shows the relationship between the applied torque and the angular deflection of the gear coupling, i.e., it reflects the stiffness of the component. It can be observed that the angular deflection increases as the misalignment angle increases. This is fundamentally based on the lower number of teeth which are transferring the applied torque.

At low misalignment angles ($\gamma < 1.5°$), the slope (Fig. 11(b)) of this trend remains quasi constant as a function of torque. Indeed, with all the teeth making contact the increase of stiffness mainly resides in the existence of a bigger contact area due to the tooth surface deformations.

As the misalignment angle increases, stiffness values are reduced. Moreover, the increase of the slope in Fig. 11(b) is observed as more teeth make contact as torque increases. For higher misalignment angles ($\gamma = 6°$ or $\gamma = 7.5°$), a quasi constant slope is not observed as torque values are not big enough so that all the teeth make contact.

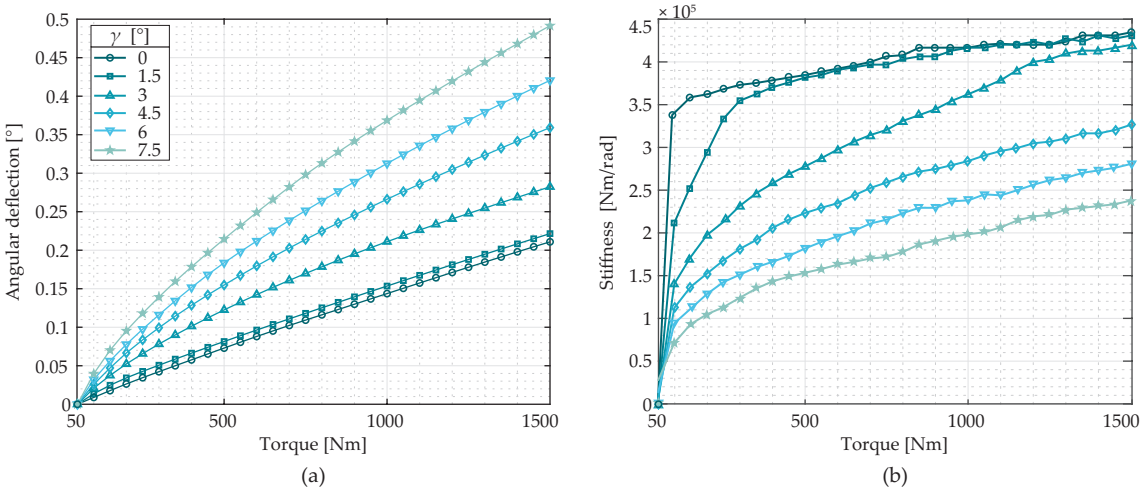

Figure 11: (a) angular deflection, and (b) stiffness of a highly crowned spherical gear coupling as a function of the applied torque.

5.2.2. Contact pattern evolution

Compared to section 5.1.1 (where all tooth positions are considered without the convective effects of adjacent teeth), the contact pattern no longer shows the lemniscata shape at high misalignment angles. What's more, the number of teeth in contact is reduced and principally located in the tilting position (most displaced positions from the reference section), as can be seen in Fig. 12. The contacting teeth centroid is represented together with the arrows showing that contact passes from one half of the active profile to the other.

The evolution of the contact pattern as a function of the applied torque or the misalignment angle is not represented for the purpose of simplicity, as it presents the same behavior as the one shown in Fig. 9 for the single teethed gear coupling.

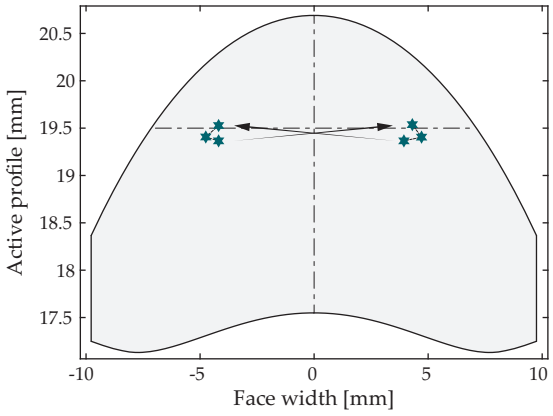

Figure 12: Contact pattern centroids for $\Gamma = 1000$ Nm and $\gamma = 6°$.

5.2.3. Load distribution

Fig. 13 describes the load distribution in terms of the misalignment angle and the applied torque (bar colors). Each set of bars refers to one of the teeth of the gear coupling. The abscissa axis shows the angular position of the tooth, while the ordinate axis represents the percentage of the total load carried by each tooth in that angular position. Pivoting and tilting positions are also marked for ease of understanding. The last set of bars is the same as the first, to represent the whole circular load distribution.

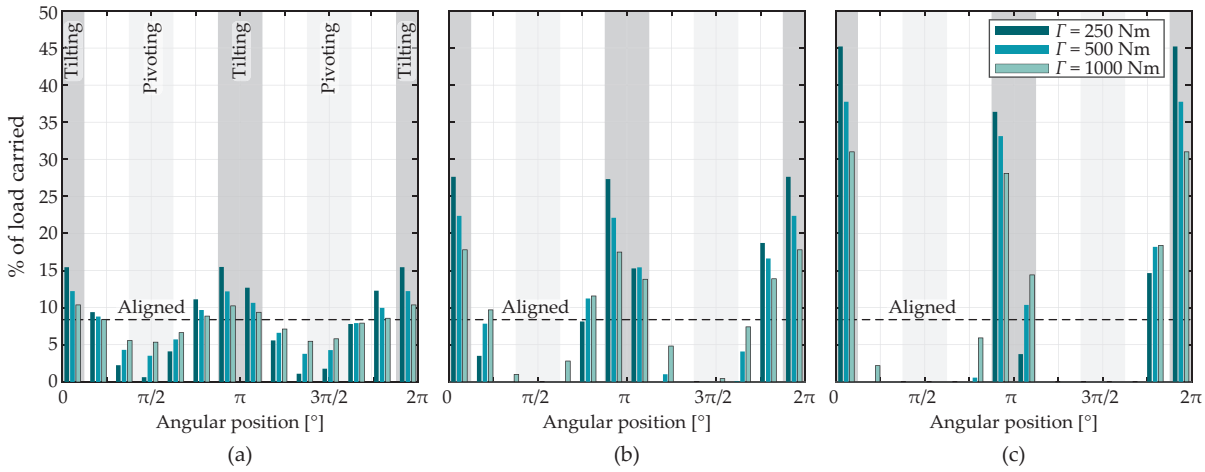

Figure 13: Effect of the applied torque and the misalignment angle (a) $\gamma = 1.5°$, (b) $\gamma = 3°$, and (c) $\gamma = 6°$ in the load distribution of a highly crowned spherical gear coupling.

It is observed that at low misalignment ($\gamma = 1.5°$) load is more evenly distributed than at higher misalignment angles, as the number of teeth in contact is higher. Moreover, it can be seen that the teeth which support the highest loads are those in the tilting positions, as they are the first entering into contact, even at low misalignment.

Furthermore, lower torques are the most critical ones in terms of load distribution, since very few teeth come into contact, i.e., the deformation caused by the torque is smaller than the angular backlash. Indeed, the load is mainly shared among three to four teeth when the misalignment angle increases. It can also be seen that the load in the tilting angular position is increased as the misalignment angle increases. At the same time, the load supported by those teeth in the pivoting angular position decreases or even loses contact as the misalignment angle increases. In addition, regardless of the misalignment angle, when torque is increased, as tooth deflections are greater than the clearance, more teeth come into contact and load distribution is more evenly shared. In this manner, the load supported by all the teeth gets closer to the aligned case: for the tilting position the supported load decreases, while for the pivoting position it increases.

To better understand the sequence in which load is distributed, Fig. 14 shows the cumulative percentage of load carried by the teeth engaged in the spherical gear coupling at different misalignment angles. The slashed line shows

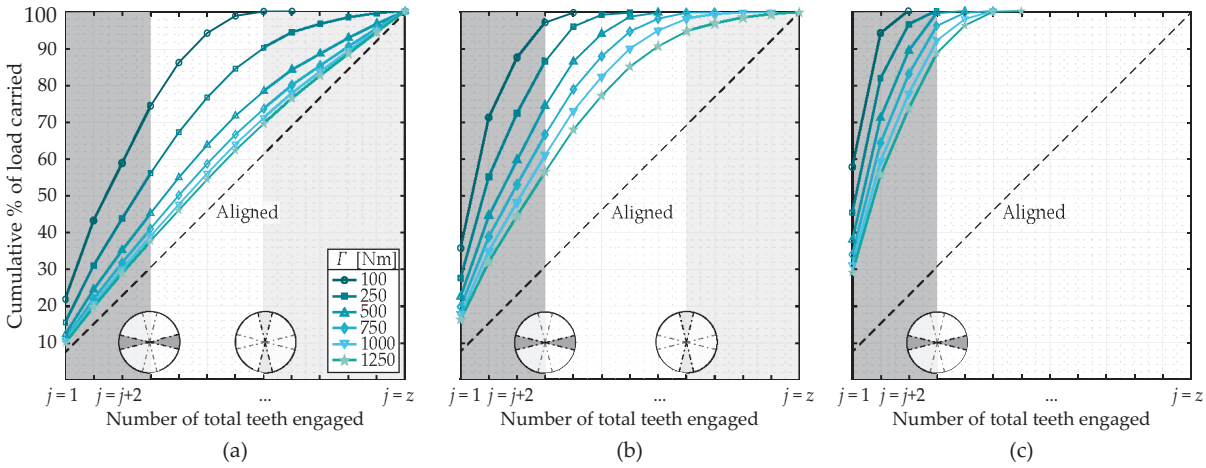

Figure 14: (a) cumulative percentage of load carried by the teeth engaged at (a) $\gamma = 1.5°$, (b) $\gamma = 3°$, and (c) $\gamma = 6°$ as a function of the applied torque.

the case of the aligned conditions where a constant slope increase can be seen, meaning an equal load distribution among all the teeth. However, in misaligned conditions, the curves no longer present a constant slope and shift away from the aligned curve as torque decreases. Moreover, as the misalignment angle increases the curves are more shifted away from the aligned case, which means fewer teeth in contact with less homogeneous load distribution.

The curves present a steep slope among the first teeth engaged (those in the tilting angular position), while as the load is spread over more teeth, the slope decreases. Indeed, this demonstrates that the last teeth engaging (those in the pivoting angular position) contribute nearly nothing to the total load transferred by the gear coupling.

5.2.4. Tooth root stresses

Maximum tooth root stress

In section 5.1.2 it is shown that the maximum tooth root stress position displaces considerably from the reference section in the presence of a misalignment angle, moving together with the contact point. In this section, the modification of the tooth root stress value due to the non-uniform load distribution among the teeth in presence of the misalignment angle is discussed.

From the load distribution analysis, it is concluded that teeth in the tilting angular position are the ones that support the highest loads, thus they are the ones suffering the highest tooth root stresses. Fig. 15(b) shows the tooth root stress distribution of the tilting angular position along the face width as a function of the misalignment angle. It depicts how as the contact centroid displaces from the reference section (Fig. 15(a)), tooth root stress distribution is no longer symmetric. It is also shown how the maximum value increases with the misalignment angle, and shifts together with the contact centroid along the face width direction.

Fig. 15(c) shows the stress distribution on the traction side of the tooth of the hub. Contact stresses are not displayed since it is not the objective of this research. It can be seen that stresses decrease drastically after the contact, which may lead to think that not all the face width of the gear coupling is supporting the load as already described in [20, 22]. Moreover, it is observed that there is no stress concentration or discontinuity when undercutting sections start, even if higher values are observed when the contact point is close to them ($\gamma = 6°$).

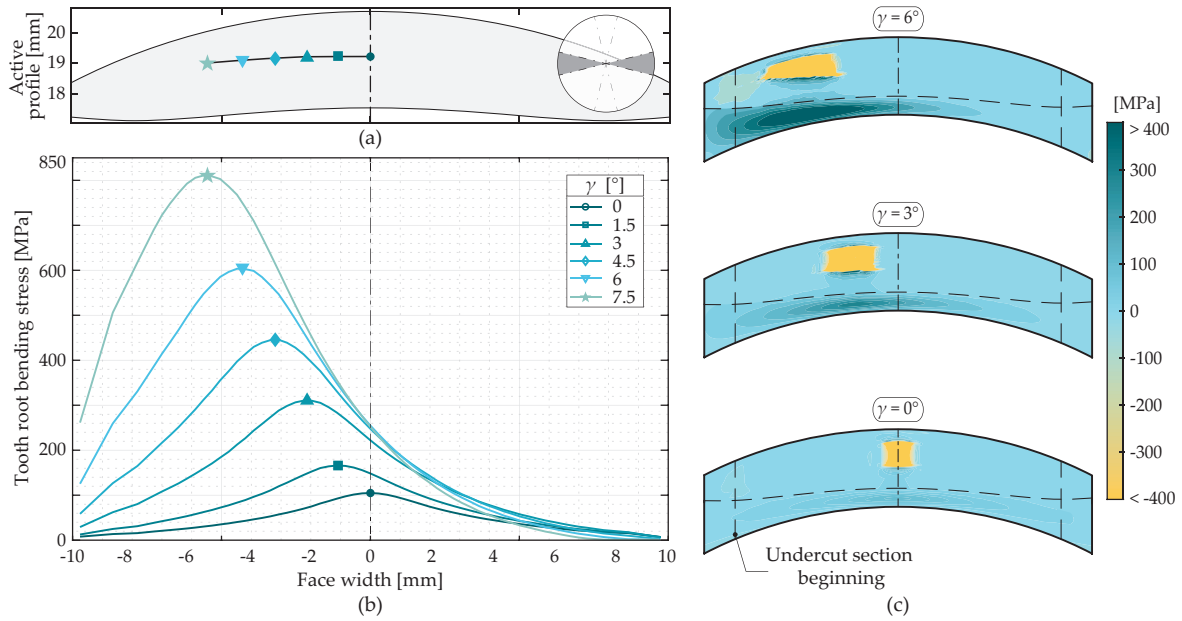

Figure 15: (a) the centroid evolution, and (b) the tooth root bending stress along the hub face width of the tilting angular position at $\Gamma = 500$ Nm in terms of the misalignment angle, together with (c) the stress distribution in the traction side of the tooth surface.

Even if the maximum tooth root stress occurs at the tilting angular position, for the aim of comparing, Fig. 16 shows the maximum stress values of (a) tilting and (b) pivoting angular positions as a function of the applied torque and the misalignment angle.

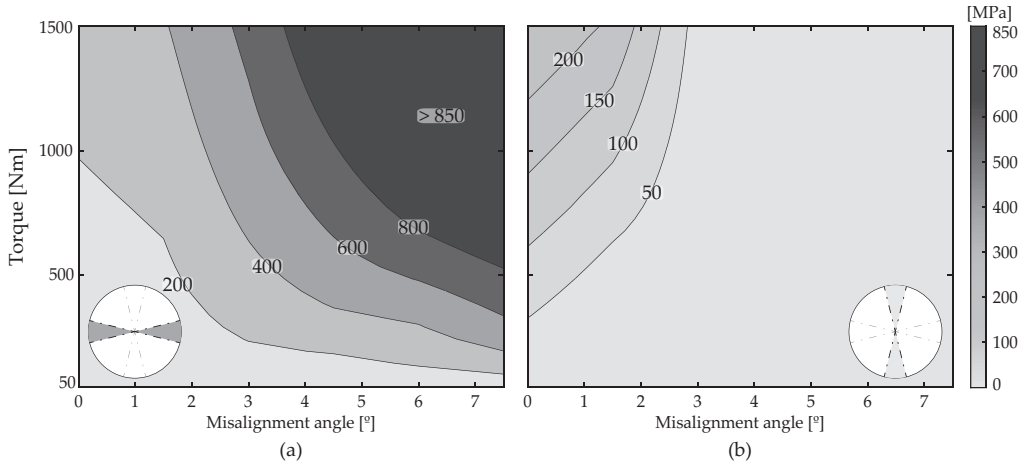

Figure 16: Maximum tooth root bending stress in terms of the applied torque and misalignment angle (a) in the tilting position, and (b) in the pivoting position.

It can be seen that stress values in pivoting angular positions are very low and do not follow the same trend as those in the tilting position. This is because, as shown in the previous section, only at low misalignment angles ($\gamma \leq 1.5°$) all the teeth in the gear coupling are in contact, and thus, as torque increases the stresses increase in either of the positions.

However, when the misalignment angle increases the number of teeth in contact decreases, especially those in the pivoting position. In consequence, the stress values in the pivoting position decrease, as teeth in the tilting position support the highest stresses. Moreover, it can be observed that for the pivoting position (Fig. 16(b)) at lower torques no stresses (due to the loss of contact) are supported by the teeth.

These results clearly remark that stress values vary significantly according to the angular position of the gear coupling and, thus, when sizing according to tooth-root fatigue it becomes very important to analyze the tooth root stress cycle.

Tooth root stress cycle

It has already been seen that the stress state at different angular positions is different. That is why, with the aim of better understanding the behavior towards fatigue tooth root breakage, Fig. 17 shows the tooth root stress evolution at various sections along the face width to analyze if the maximum stresses are always located at the same section. The different positions shown in Fig. 17 at a constant torque of 500 Nm are: (a) the reference section, (b) the contact section in the tilting position which varies together with the misalignment angle, and (c) the undercut beginning section.

It is observed that the highest bending stresses occur in the contact (Fig. 17(b)) and in the undercutting (Fig. 17(c)) sections at the tilting position. For the case of the undercutting section, it is seen that stresses along the cycle are very low and close to the value of the aligned case. Indeed, it is shown that tilting positions are a stress concentration location along the cycle, which will need to be considered especially when the contact point displaces due to the misalignment angle nearby the undercutting section (e.g., see stress value increase between the contact section and the undercutting section at 0 rad for $\gamma = 7.5°$).

With regard to the contact section (Fig. 17(b)), the stress cycle is also characterized by the peak values in the tilting position, while it is more homogeneous along the rest of the cycle at low misalignment angles. At high misalignment angles, stress values in parts of the cycle (i.e., pivoting positions) are null since the teeth lose contact.

Concerning the reference section (Fig. 17(a)) of the gear hub, the stress cycle is close to that of the contact section, while it does not present so high values in the tilting position. Moreover, it can also be seen that in each revolution, a tooth will pass twice through each stress state. However, when getting closer to the edges of the gear coupling (e.g., the undercutting section) it can be observed that in each revolution there is just one stress cycle. In consequence, this is another reason why the spherical gear coupling bending fatigue differs from what has been previously described in the literature.

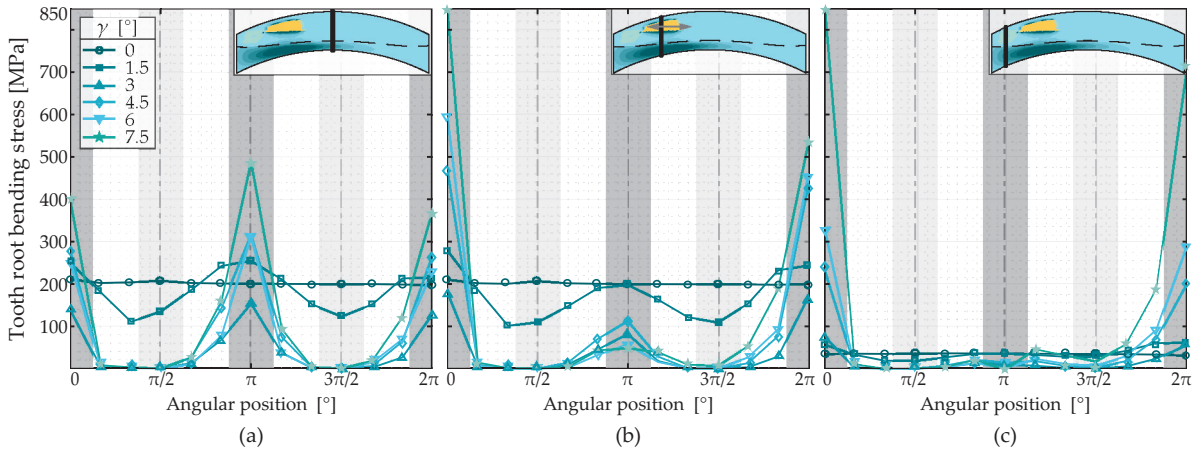

Figure 17: Maximum tooth root bending stress cycle at $\Gamma = 500$ Nm at: (a) the reference section, (b) the contact section in tilting position, and (c) the undercut beginning section.

Since the mechanical behavior varies considerably from section to section, Fig. 18(a) presents the general case of maximum tooth root bending stresses to examine the fatigue cycle endured by the gear coupling hub. The maximum stress values are in the tilting position and the lower (or even null) in the pivoting positions. Moreover, the double cycle supported by the gear coupling in each revolution is observed. Indeed, each tooth will pass twice through each position in each revolution.

According to this cycle, Fig. 18(b) and (c) represent the mean and alternating stress level of the cycle in terms of the applied torque and misalignment angle. In these graphs, two different trends can be observed (divided with a slash and dotted line). The first behavior is up to $\gamma \leq 1.5°$, where a sinusoidal fluctuating stress cycle is observed (positive fatigue stress ratio, $R > 0$). Here, teeth do not completely lose contact in any angular position, and stress values oscillate around the stress value of the aligned case.

The second behavior arises from $\gamma > 1.5°$, where teeth lose contact in the pivoting position, thus stresses descend to zero in those angular positions. This produces a repeated tensile (or pulsating tension) stress cycle ($R = 0$). This pulsating stress cycle has not been previously discussed in the literature related to gear coupling tooth root fatigue analysis, and hence, this work highlights that the behavior is more complex and that it needs a deeper understanding.

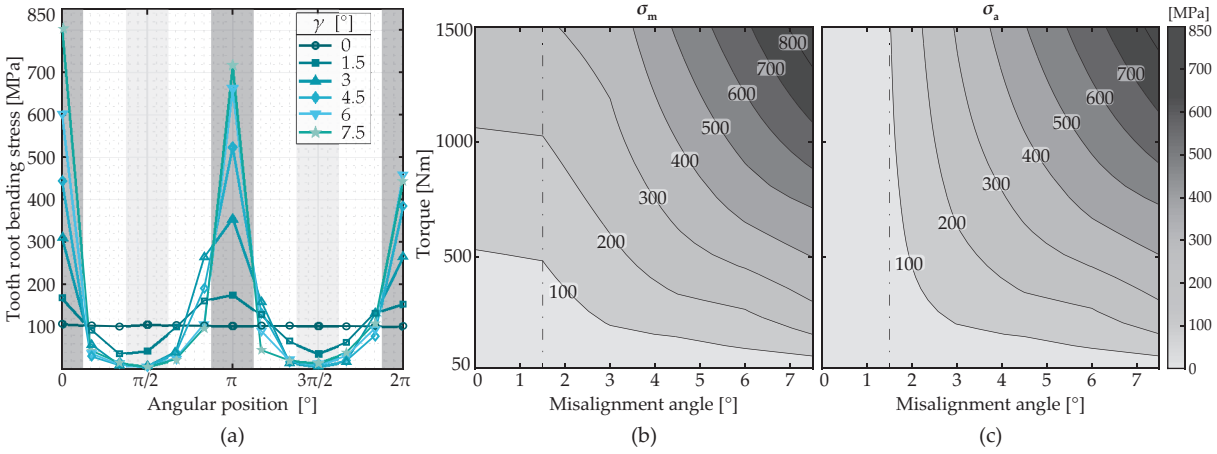

Figure 18: (a) maximum tooth root bending stress cycle of a gear coupling at $\Gamma = 500$ Nm in terms of the misalignment angle, (b) the mean, and (c) the alternating stress level in terms of the applied torque and the misalignment angle.

6. Discussion

Spherical gear couplings working at high misalignment angles have shown to have a very complex and different mechanical behavior from what has been previously analyzed in the specialized literature. From the tooth root sizing equations described in the introduction, the importance of two coefficients to account for the influence of the misalignment angle was shown: the load sharing factor (k_{ls}), and the load distribution factor (k_m). In the following paragraphs, the influence of both coefficients will be discussed based on the results obtained from the loaded tooth contact analysis.

Concerning the load sharing factor, one of the most remarkable aspects of highly crowned spherical gear couplings working at high misalignment angles is the reduction of the number of teeth in contact depending on the working conditions (Γ and γ). Furthermore, it has also been seen that not all the teeth support the load equally, which is in agreement with some works of the literature [22, 34, 62]. Indeed, due to the non-uniformity of the load distribution, knowing the number of teeth in contact is sometimes not sufficient to determine the maximum tooth root stresses. That is why some authors [34, 62, 63] propose determining the effective number of teeth in contact (C_{eff}), or which is equivalent the overload coefficient (k_F). This is defined following Eq. (14), and is a more representative value than the number of teeth in contact since it considers the number of teeth which are really transferring the load. This value is obtained by dividing the average load supported by each tooth (Γ_{avg_j}), and the load carried by the most charged one (Γ_{max_j}). For instance, in aligned conditions $C = C_{\text{eff}}$, that is $k_F = 1$, meaning all the teeth are equally loaded.

$$C_{\text{eff}} = \frac{\Gamma_j}{\Gamma_{\text{max}_j}} = \frac{\Gamma/z}{\Gamma_{\text{max}_j}} = \frac{1}{k_F} = \frac{1}{k^*_{ls}} \tag{14}$$

In Fig. 19, both, the number of teeth (a) and the effective number of teeth (b) are shown. It can be seen that as the applied torque decreases and the misalignment angle increases, the number of teeth in contact decreases drastically. Moreover, it is observed that even if in applications with $\gamma \leq 2°$ and $\Gamma \geq 800$ Nm all the teeth are in contact (Fig. 19(a)), only the 80% of them are transferring the charge (Fig. 19(b)). Furthermore, working conditions with less than 20% of their teeth carrying the load is wide. This will imply tooth root stresses which can be more than five times higher than those supported under aligned conditions.

The commonly used criteria in the literature for sizing is considering that half of the teeth are in contact, regardless of the geometry or working conditions [14, 22, 42]. In Fig. 19 this value is highlighted, and it is clearly depicted that this criterion is very conservative when applied to low misalignment angles. However, for higher misalignment angles

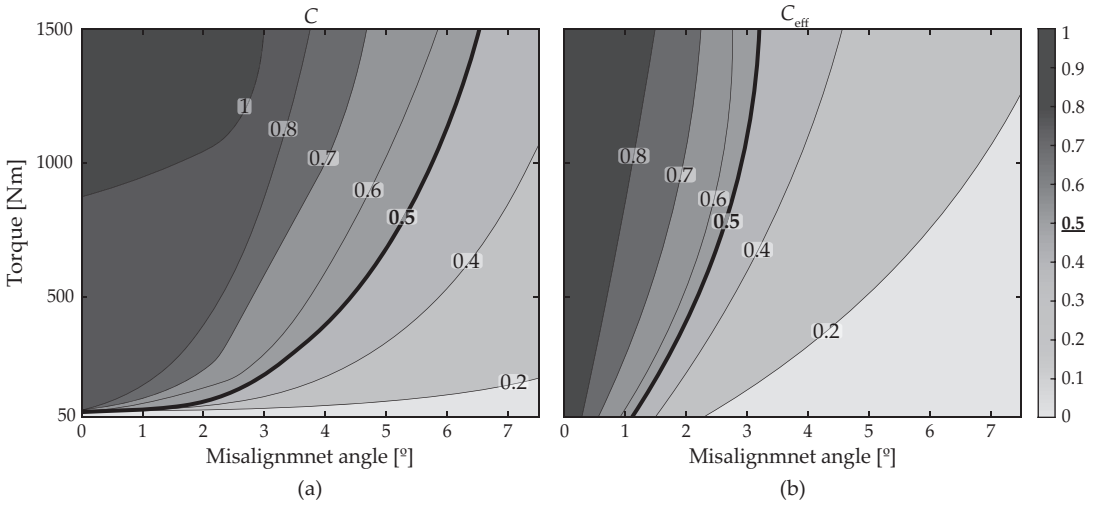

Figure 19: (a) number of teeth in contact C, and (b) effective number of teeth in contact C_{eff} as a function of the applied torque and the misalignment angle compared to the criterion of half of the teeth in contact [14].

(especially in lower torques), this criterion undersize the component, which may lead to non-compliance with the

technical requirements or premature failure. It can be observed that the undersized area is greater if the effective number of teeth is considered, concluding that C_{eff} is a parameter that must be taken into account during sizing.

AGMA 945 B20 [22] hard codes a value of 2 or 3 for the load sharing coefficient giving as a reference the criteria of half of the teeth carrying the load, thus in this work the overload coefficient k_F is defined to substitute it in the sizing equation by the k^*_{ls} coefficient.

On the other hand, concerning the load distribution factor, another remarkable behavior of highly crowned gear couplings working at high misalignment angles is the displacement of the contact point along the face width of the active profile. The contact point and the contact pattern are in agreement with the literature [29, 30, 31]. Nevertheless, these works were oriented to low misalignment angles $\gamma \ll 1^\circ$ and geometries with high crowning radius (i.e., low longitudinal crowning), thus they had a high risk of edge or tip contact. To avoid this problem, the use of a tip relief has yielded satisfactory results in this research, even if further research is required to obtain the most optimized value.

Referring to the maximum displacement along the face width, Fig. 20 compares the values obtained in this research with those calculated with the equation from the literature (Eq. (2)) [11, 32]. It is observed that the maximum displacement of the contact point ($\delta_{\max}$) is largely increased with the misalignment angle (torque has a negligible effect). Fig. 20 shows that differences between the LTCA and the literature are very relevant and that the literature values remain way lower. Indeed, these equations make simplifications in the geometrical parameters, as they are developed for geometries with low values of longitudinal crowning.

Thereby, there is a major displacement of the contact during the operation of a highly crowned spherical gear coupling compared to those commonly used in quasi-aligned conditions. Indeed, there will be an increase in the entrainment velocity thanks to which lubricant will properly flow across the tooth surfaces. In short, fretting wear will no longer be the main failure mechanism, and thus, tooth root fatigue failure should be analyzed to avoid component breakage.

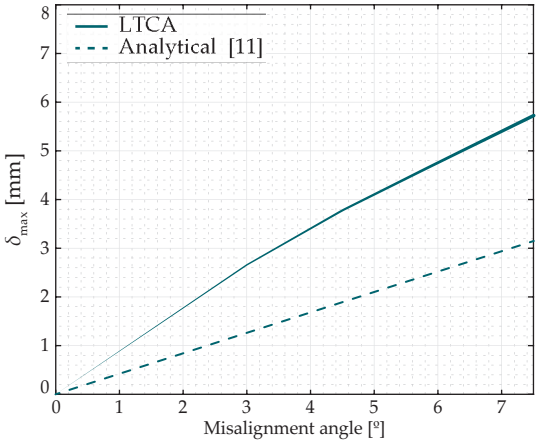

Figure 20: Maximum contact position displacement amplitude for highly crowned spherical gear couplings compared with [11] Eq. (2).

In AGMA 945 B20 [22] the load distribution factor is obtained dividing the face width by the amplitude of the contact pattern. However, this might not be an appropriate definition for highly crowned hubs, as they give higher coefficients at aligned than at misaligned conditions. Indeed, as shown in Fig. 20 the contact pattern amplitude ($2\delta_{\max}$) increases with the misalignment angle. For that reason, in this work, it is suggested to define the effective face width b_{eff} by calculating the length of the face width that is bearing stresses above the 70% of the maximum tooth root bending stress ($0.3\,\sigma_{\max}$), as shown in Fig. 21(a). According to the figure, it can be observed that as the misalignment angle increases the effective face width does not significantly vary for a constant torque (e.g., $b_{\text{eff}} = 10.4$ mm for $\gamma = 6^\circ$, while $b_{\text{eff}} = 11$ mm for $\gamma = 1.5^\circ$). In Fig. 21(b) it is indeed observed that the normalized effective face width trends are close to the same values at high torque values. Different behavior for the case of $\gamma = 7.5^\circ$ is observed, which may be linked to the excessive displacement of the contact point compared to the face width of the case study. These results suggest that the effective face width is a parameter linked principally to the gear hub geometry, and not highly dependent on the misalignment angle.

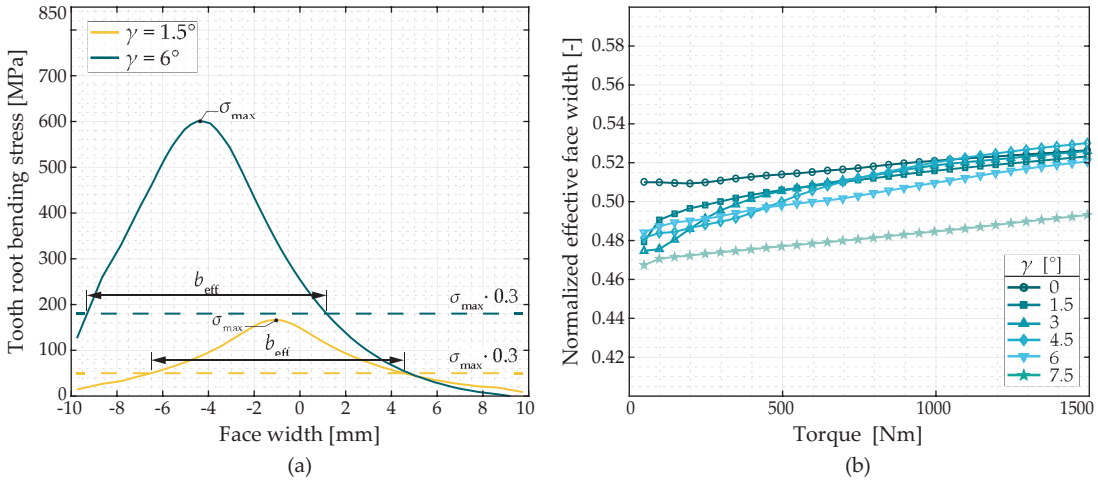

Figure 21: (a) suggested definition of the effective face width (b_{eff}) for highly crowned gear couplings, and (b) normalized b_{eff} evolution as a function of the applied torque and the misalignment angle.

In consequence, a modified load distribution coefficient (k_m^*) is defined to use it in the tooth root stress equation, considering the effective face width results (Eq. (15)). As depicted in Fig. 21(b), values for all the misalignment angles but that from 7.5° gather around $b_{\text{eff}} \approx 10$ mm, which corresponds to a load distribution coefficient of $k_m^* \approx 2$.

$$k_m^* = \frac{b}{b_{\text{eff}}} \tag{15}$$

With k_m^* and k_{ls}^* coefficients already re-defined by the authors, bending tooth root stress is calculated based on [22] with Eq. (16).

$$\sigma = k_a\, k_m^*\, k_{ls}^*\, \frac{2000\,\Gamma}{d_p^2\, b\, Y} \tag{16}$$

Fig. 22(a) shows LTCA results at low and high misalignment angles against those obtained with [22] and its coefficients. Leaving aside the application factor ($k_a = 1$), the load sharing (k_{ls}) and load distribution (k_m) coefficients were defined following the recommendations of the standard. Even if the standard does not give coefficient values for such high misalignment angles, the most critical from those proposed were chosen.

From these results, it can be seen that even at low misalignment angles significant differences emerge, and undersize the stresses suffered by the component. This indicates one more time that the definition of the coefficients in the standard is not accurate enough to represent the mechanical behavior of highly crowned spherical gear couplings. It is indeed concluded that sizing spherical gear couplings working in high misalignment angles can result in a premature breakage of the component, due to the undersized results obtained with the current standard.

By contrast, Fig. 22(b) shows the results obtained with Eq. (16), where, k_m^* and k_{ls}^* factors are changed according to the results obtained with the LTCA. k_m^* is adjusted with the effective face width, and k_{ls}^* factor is based on the overload coefficient k_F, i.e., the effective number of teeth in contact ($k_{ls}^* = k_F = 1/C_{\text{eff}}$). It is observed, that calculated values are very close to those from the LTCA at low or high misalignment angles. The difference is below the 10% at $\gamma = 6°$ from $\Gamma = 200$ Nm onward; e.g., at 250 Nm LTCA gives 442.5 MPa, while those obtained with the modified coefficients in the standard gives 403.7 MPa.

That is why it is concluded that tooth root bending stress of highly crowned spherical gear couplings working at high misalignment angles can be accurately represented with a deeper analysis in the determination of the load sharing and load distribution factors. This analysis, among others, will enable ensuring a common and accurate procedure to determine tooth root stress of spherical gear couplings working at low or high misalignment angles.

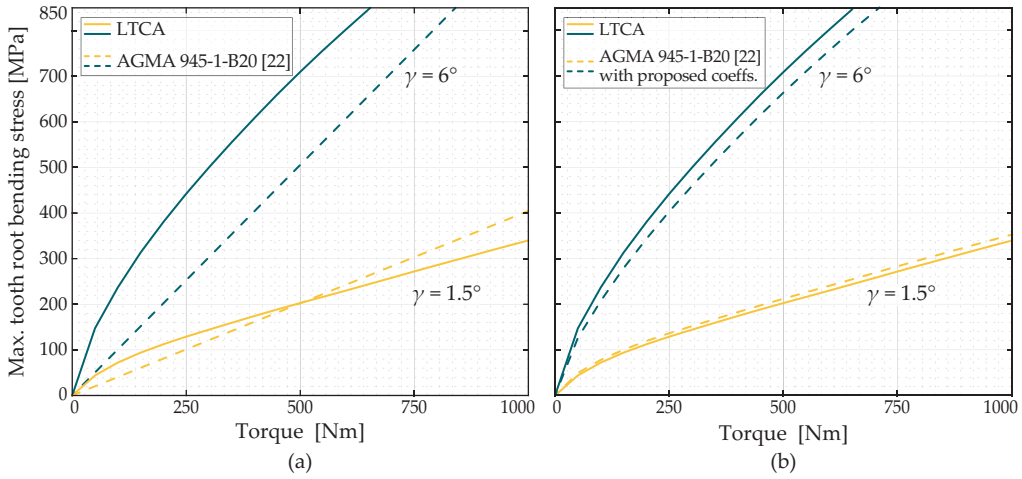

Figure 22: Comparison of the maximum tooth root bending stress at $\gamma = 1.5°$ and $\gamma = 6°$: (a) between LTCA and [22], and (b) between LTCA and [22] with the proposed coefficients k_m^* and k_{ls}^* deduced from LTCA results.

7. Conclusions

This paper describes the mechanical behavior of highly crowned spherical gear couplings and the influence of the operating conditions by means of a FE model developed for this purpose. The research aims to provide a more accurate definition of the influencing variables when working at high misalignment angles, to enable non-oversized and competitive designs of spherical gear couplings. Moreover, the model presented here can be easily adapted to different geometries or working conditions.

From the LTCA and the comparison with the literature the following conclusions can be drawn:

(1) The number of teeth in contact decreases drastically to less than 40% of the total number of teeth of the gear coupling at low torque values and high misalignment angles $\gamma > 3°$. As a result, the stiffness of the component is reduced and tooth root stresses are increased considerably.

(2) In addition to the decrease in the number of teeth in contact, the misalignment angle induces a non homogeneous load distribution among those in contact.

(3) Tooth root bending stresses are influenced by the contact position variation in as much as 10% of the load supported.

(4) The stress state between tilting and pivoting angular positions changes considerably at high misalignment angles, which leads to a complex tooth root fatigue life. Due to the loss of contact of some of the teeth at high misalignment angles, the fatigue cycle changes from a sinusoidal fluctuating stress cycle ($\gamma \leq 1.5°$) to a pulsating tension stress cycle ($\gamma > 1.5°$). Consequently, the fatigue life of the component might be reduced.

(5) Sizing highly crowned spherical gear couplings to tooth root breakage with actual standards may lead to under sizing in some working conditions. As a consequence, an early breakage of the component and an increase in maintenance costs are expected.

(6) The bending tooth root stresses may be accurately predicted with a proper definition of the load distribution and the load sharing coefficients. To this end, it is essential to correctly define the effective face width and the overload coefficient.

(7) The contact pattern of highly crowned spherical gear couplings working at high misalignment angles spreads over more than 50% of the face with. This leads to adequate lubrication of the component, and thus decreases wear and fretting fatigue fracture risk of this type of component.

The proposed model allows for future work to focus on the influence of different design parameters, such as the pitch diameter, the number of teeth, the pressure angle or the aspect ratio in the load distribution, and the tooth root stress of highly crowned spherical gear couplings. Moreover, this will enable further understanding of the tooth root fatigue cycle. Finally, this analysis will enable a more accurate definition of the load distribution and the load sharing coefficients, taking into account the effect of the design parameters, and making it possible to obtain the proper value for sizing coefficients.

References

[1] J. R. Mancuso, Couplings and joints: design, selection and application, Technology & Engineering. M. Dekker, 1986.

[2] S. Hahn, Coupling connections and splines, in: Encyclopedia of Automotive Engineering, John Wiley & Sons, 2014, pp. 1–14. doi:10.1002/9781118354179.auto094.

[3] W. Herbstritt, J. Paluh, Mill spindle advanced gear design, Iron and Steel Engineers 76 (7) (1999) 44–48.

[4] P. Krot, Transient torsional vibrations control in the geared drive trains of the hot rolling mills, in: IEEE International Conference on Control Applications, St. Petersburg, 2009, pp. 1368–1373. doi:10.1109/CCA.2009.5280933.

[5] I. Ulacia, J. Larrañaga, A. Arana, A. Iñurritegui, J. Elizegi, Fatigue life prediction of spherical gear couplings, in: American Gear Manufacturers Association Fall Technical Meeting 2018, Illinois, 2018, pp. 202–207.

[6] F. Ohshima, S. Hirata, H. Yoshino, Study on tooth contact of gear couplings, Transactions of the Japan society of mechanical engineers. Series C 78 (786) (2012) 639–649. doi:10.1299/kikaic.78.639.

[7] Y. Guan, X. Yang, Z. Fang, G. Chen, Comparative analysis of three geometric models for crown gear coupling, Mechanism and Machine Theory 136 (2019) 269–283. doi:10.1016/j.mechmachtheory.2019.02.016.

[8] A. Iñurritegui, I. Gonzalez-Perez, A. Arana, J. Larrañaga, I. Ulacia, Computerized generation and tooth contact analysis of spherical gear couplings for high misalignment applications, Mechanism and Machine Theory 164 (2021). doi:10.1016/j.mechmachtheory.2021.104408.

[9] P. Ku, M. Valtierra, Spline wear-effects of design and lubrication, Journal of Engineering for Industry 97 (4) (1975) 7. doi:10.1115/1.3438738.

[10] S. Medina, A. V. Olver, Regimes of contact in spline couplings, Journal of Tribology 124 (2) (2002) 351–357. doi:10.1115/1.1403456.

[11] Y. Guo, S. Lambert, R. Wallen, R. Errichello, J. Keller, Theoretical and experimental study on gear-coupling contact and loads considering misalignment, torque and friction influences, Mechanism and Machine Theory 98 (2016) 242–262. doi:10.1016/j.mechmachtheory.2015.11.015.

[12] L. Xiao, Y. Xu, X. Sun, H. Xu, L. Zhang, Experimental investigation on the effect of misalignment on the wear failure for spline couplings, Engineering Failure Analysis 131 (2022). doi:10.1016/j.engfailanal.2021.105755.

[13] S. Locke, M. Burgess, S. Steve, W. Virginia, J. Corcoran, T. Hess, J. Joe, T. Hess, Coupling credible failure modes and owner options to intervene, in: 42th Turbomachinery Symposium, Texas, 2013, pp. 1–30.

[14] D. Dudley, When splines need stress control, Product Engineering 28 (1957) 56–59.

[15] X. Xue, Q. Huo, L. Hong, Fretting wear-fatigue life prediction for aero-engine's involute spline couplings based on Abaqus, Journal of Aerospace Engineering 32 (6) (2019) 04019081. doi:10.1061/(asce)as.1943-5525.0001058.

[16] S. Leen, Fretting fatigue and wear of spline couplings: from laboratory testing to industrial application through computational modelling, in: Wear in advanced engineering applications and materials, World Scientific, 2022, pp. 1–44. doi:10.1142/9781800610699.

[17] Y. Guan, J. Chen, Z. Fang, S. Hu, A quick multi-step discretization and parallelization wear simulation model for crown gear coupling with misalignment angle, Mechanism and Machine Theory 168 (2022). doi:10.1016/j.mechmachtheory.2021.104576.

[18] Z. Ye, Z. Chen, H. Lu, S. Wang, Z. Li, M. Yang, W. Wu, Analysis of parallel misalignment of gear coupling in rotor system using EEMD-median filter method, IEEE Advanced Information Technology, Electronic and Automation Control Conference (IAEAC) 2021 (1) (2021) 1113–1118. doi:10.1109/IAEAC50856.2021.9390976.

[19] A. Iñurritegui, A. Arana, J. Larrañaga, I. Ulacia, Spherical gear coupling design space analysis for high misalignment applications, Mechanism and Machine Theory 173 (2022) 104837. doi:10.1016/j.mechmachtheory.2022.104837.

[20] Deutsches Institut für Normung, DIN 5466: Splined joints, calculation of load capacity (2002).

[21] International Organization for Standardization, ISO 4156: Straight cylindrical involute splines (2005).

[22] American Gear Manufacturers Association, AGMA 945-1-B20: Splines – Design and Application (2020).

[23] R. Beckmann, Beitrag zur Auslegung und Konstruktion von Balligzahn-Kupplungen, Ph.D. thesis, Chemmitz Technology University (2005).

[24] R. Cedoz, M. Chaplin, Design guide for involute splines, Society of Automotive Engineers, 1994.

[25] M. Octrue, F. Blanc, D. Ghribi, Guide de demensionnement des accouplements à dentures bombées, CETIM, 2014.

[26] J. Hong, D. Talbot, A. Kahraman, Load distribution analysis of clearance-fit spline joints using finite elements, Mechanism and Machine Theory 74 (2014) 42–57. doi:10.1016/j.mechmachtheory.2013.11.007.

[27] E. Neale, Introduction to gear couplings, Tech. rep., Neale consulting engineers (1980).

[28] F. Paddon, Application and selection of gear type spindles, Iron and Steel Engineer (1960) 91–100.

[29] M. Alfares, A. Falah, A. Elkholy, Clearance distribution of misaligned gear coupling teeth considering crowning and geometry variations, Mechanism and Machine Theory 41 (10) (2006) 1258–1272. doi:10.1016/j.mechmachtheory.2005.11.004.

[30] Y. Guan, Z. Fang, X. Yang, G. Chen, Tooth contact analysis of crown gear coupling with misalignment, Mechanism and Machine Theory 126 (2018) 295–311. doi:10.1016/j.mechmachtheory.2018.04.019.

[31] K. Nakashima, Teeth contact behaviour and load distribution of gear couplings, Trans. Jpn. Soc. Mech. Eng. 502 (Part C 54) (1988) 1302–1307. doi:10.1299/kikaic.54.1302.

[32] F. Curà, A. Mura, Theoretical and numerical evaluation of tilting moment in crowned teeth splined couplings, Meccanica 53 (1-2) (2018) 413–424. doi:10.1007/s11012-017-0730-1.

[33] J. Larrañaga, A. Arana, I. Ulacia, J. Esnaola, I. Torca, Misalignment effect on contact pressure and tooth root strength of spline couplings, in: 5th International Conference on Power Transmission-BAPT, Ohrid, Macedonia, 2016, pp. 1–6.
[34] J. Silvers, C. Sorensen, K. Chase, A new statistical model for predicting tooth engagement and load sharing in involute splines, AGMA - 10FTM07 (2010). doi:978-1-55589-982-0.
[35] K. Chase, C. D. Sorensen, B. J. DeCaires, Variation analysis of tooth engagement and loads in involute splines, IEEE Transactions on Automation Science and Engineering 7 (4) (2010) 746–754. doi:10.1109/TASE.2009.2033033.
[36] C. Bünder, Analyse der Beanspruchungen der Verzahnung von Zahnkupplungen, Ph.D. thesis, Technische Universität Dresden (2000).
[37] J. Hong, D. Talbot, A. Kahraman, Effects of tooth indexing errors on load distribution and tooth load sharing of splines under combined loading conditions, Journal of Mechanical Design (2015). doi:10.1115/1.4029282.
[38] M. Benatar, D. Talbot, A. Kahraman, An experimental investigation of the load distribution of spline joints under gear loading conditions, Journal of Advanced Mechanical Design 11 (6) (2017) 1–12. doi:10.1299/jamdsm.2017jamdsm0084.
[39] F. Curà, A. Mura, M. Gravina, Load distribution in spline coupling teeth with parallel offset misalignment, Proceedings of the Institution of Mechanical Engineers, Part C: Journal of Mechanical Engineering Science 227 (10) (2013) 2195–2205. doi:10.1177/0954406212471916.
[40] P. Renzo, S. Kaufman, D. de Rocker, Gear couplings, Journal of Engineering for Industry (1968) 467–474.
[41] S. Lagutin, B. Utkin, A. Klochkov, Upgrading of the geometry of gear couplings, in: 7th International KOD Symposium, Hungary, 2012, pp. 27–30.
[42] G. Henriot, J. Boisset, Accouplements, alignement des axes, in: Engrenages: conception, fabrication, mise en oeuvre, 5th Edition, Dunod, 1983, pp. 796–818.
[43] B. Volfson, Stress sources and critical stress combinations for splined shaft, Journal of Mechanical Design 104 (1) (1982) 551–556. doi:10.1115/1.3256385.
[44] A. Elkholy, M. Alfares, Misalignment loads in splined gear couplings, International Journal of Computer Applications in Technology 15 (1-3) (2002) 128–137. doi:10.1504/IJCAT.2002.000288.
[45] Z. Kahn, S. Wright, Finite element analysis of an involute spline, Journal of Mechanical Design 122 (2) (2000) 239. doi:10.1115/1.533573.
[46] J. Kroczak, M. Dudziak, Analysis of the pitch deviation in involute splined connections, Machine Dynamics Research 37 (1) (2013) 65–71.
[47] D. Marano, M. Lorenzini, L. Mastrandrea, F. Pulvirenti, M. Turci, N. Fillault, Misalignment compensation spline design, in: American Gear Manufacturers Association Fall Technical Meeting 2019, Dallas, 2019, pp. 1–17.
[48] R. Vondra, K. Rehak, A. Prokop, Strain-stress analysis of gear coupling, Engineering Mechanics 2020 26 (2020) 520–523. doi:10.21495/5896-3-520.
[49] C. Dupertuis, J. Ligier, Contact pressure in misaligned spline couplings, Mechanics and Industry 21 (5) (2020). doi:10.1051/meca/2020049.
[50] Y. Guan, Z. Fang, X. Yang, G. Chen, Effects of misalignment and crowning on contact characteristics of crown gear coupling, Journal of Mechanical Engineering Science 0 (0) (2018).
[51] J. Wei, Y. Yao, K. Zhang, Contact analysis and surface optimization of crowning gear coupling, in: Proc. of the 2nd International Conference on High Performance and Optimum Design of Structures and Materials, Vol. 166, 2016, pp. 455–465. doi:10.2495/HPSM160421.
[52] R. Heinz, Untersuchung der Kraft- und Reibungsverhältnisse in Zahnkupplungen für grobe Leistungen, Ph.D. thesis, TU Darmstadt (1977).
[53] J. Pedrero, M. Pleguezuelos, M. Sánchez, Load sharing model for high contact ratio spur gears with long profile modifications, Forschung im Ingenieurwesen 83 (3) (2019) 401–408. doi:10.1007/s10010-019-00379-w.
[54] X. Xu, Y. Liang, S. Zuo, P. Tenberge, P. Dong, Y. Liu, S. Wang, Z. Wang, A novel tooth tip relief method for reducing micro-pitting of spur gears, Advances in Mechanical Engineering 13 (9) (2021) 1–14. doi:10.1177/16878140211044641.
[55] F. Litvin, A. Fuentes, Gear geometry and applied theory, 2nd Edition, Cambridge University Press, 2004.
[56] J. Argyris, A. Fuentes, F. Litvin, Computerized integrated approach for design and stress analysis of spiral bevel gears, Computer Methods in Applied Mechanics and Engineering 191 (11-12) (2002) 1057–1095.
[57] I. Gonzalez-Perez, A. Fuentes, Implementation of a finite element model for gear stress analysis based on tie-surface constraints and its validation through the Hertz's theory, Journal of Mechanical Design, Transactions of the ASME 140 (2) (2017) 1–13. doi:10.1115/1.4038301.
[58] MSC.Software, Marc 2019 - Volume B: Element Library (2019).
[59] K. Fujita, F. Obata, K. Miyanishi, Gear tooth stress calculation method for heavily crowned gear, Bulletin of the JSME 17 (104) (1974).
[60] K. Wesolowski, Dreidimensionale Beanspruchungszustaande und Festigkeitsnachweis drehmomentbelasteter Zahnwellen-Verbindungen unter elastischer und teilplastischer Verformung, Ph.D. thesis, TIB Hannover, Düsseldorf (1997).
[61] MSC.Software, Marc 2019 - User's Guide (2019).
[62] B. De Caires, Variation analysis of involute spline tooth contact, Ph.D. thesis, Brigham Young University (2006).
[63] J. Cavaillès, F. Groix, Etude de la répartition de la charge appliquée sur un accouplement délignable à petites dents fonctionnant en position délignée, Bulletin de l'Association Technique Maritime et Aéronautique (1971).